Physica Scripta. Vol. 59, 286–295, 1999

Relativistic Many-Body Calculations of Transition Probabilities for the $2l_1 2l_2[LSJ] - 2l_3 2l_4[L'S'J']$ Lines in Be-like Ions

U. I. Safronova, W. R. Johnson, M. S. Safronova and A. Derevianko

Department of Physics, University of Notre Dame, Notre Dame, IN 46556, USA

Received August 10, 1998; accepted October 17, 1998

PACS Ref: 32.70.Cs, 31.15.Md, 31.25.-v, 31.30.Jv

Abstract

Reduced matrix elements, oscillator strengths, and transition rates are calculated for all allowed and forbidden 2s–2p electric dipole transitions in berylliumlike ions with nuclear charges ranging from $Z = 4$ to 100. Many-body perturbation theory (MBPT), including the Breit interaction, is used to evaluate retarded E1 matrix elements in length and velocity forms. The calculations start with a $1s^2$ Dirac–Fock potential and include all possible $n = 2$ configurations, leading to 4 odd-parity and 6 even-parity states. First-order perturbation theory is used to obtain intermediate coupling coefficents. Second-order MBPT is used to determine the matrix elements, which are evaluated for the 16 possible E1 transitions. The transition energies used in the calculation of oscillator strengths and transition rates are evaluated using second-order MBPT. The importance of virtual electron–positron pair (negative energy) contributions to the transition amplitudes is discussed.

1. Introduction

Numerous theoretical and experimental studies of oscillator strengths and transition probabilities for $2s^2$–2s2p and 2s2p–$2p^2$ transitions along the beryllium isoelectronic sequence have been made during the past 30–40 years. Z-expansion [1–7], model potential [8–10], configuration interaction (CI) [11–19], multiconfiguration Hartree–Fock (MCHF) [20–26], R-matrix [27, 28], and multiconfiguration Dirac–Fock (MCDF) [29–35] methods have been used to determine transition rates in Be-like ions.

Nonrelativistic perturbation theory (the Z-expansion method) was used in early calculations to determine first- and second-order dipole matrix elements for allowed $2s^a2p^b$–$2s^{a-1}2p^{b+1}$ transitions. The earliest nonrelativistic values of the second-order dipole matrix elements were given by Cohen and Dalgarno [1], and by Dalgarno [3] in the Hartree–Fock (HF) approximation. Later, Safronova *et al.* [2] included correlation contributions to these matrix elements. It should be noted that the mixing of quasi-degenerate configurations ($2s^22p^b + 2p^{b+2}$) was included in all results obtained by the Z-expansion method [1–7]. Relativistic corrections were included perturbatively in some of these calculations [4–7] and it was recently shown [6] that the Z-expansion method with relativistic corrections gives accurate data for Be-like ions with $6 \leqslant Z \leqslant 54$.

Relativistic wave functions were used to calculate oscillator strengths for Be-like ions by Kim and Desclaux [29] and by Armstrong, Fielder, and Lin [30]. These wave functions were obtained from multiconfiguration Dirac–Hartree–Fock (MDHF) calculations including $2s^2$ and $2p^2$ configurations. Two electromagnetic gauges which in the nonrelativistic limit give the length and velocity forms for the transition operator were used in [30]. Disagreements between length and velocity f-values were found for $2s^2\,{}^1S_0$–$2s2p\,{}^1P_1$ and $2s^2\,{}^1S_0$–$2s2p\,{}^3P_1$ transitions. Even for $Z = 92$, f-values in the length and velocity forms differed by 5%. It should be noted that the nonrelativistic length and velocity f-values (also calculated in [30]) agreed much better than relativistic ones. It was shown by Cheng and Johnson [31] that the disparity between length- and velocity-form results in the MCDF calculations was due in part to neglect of "exchange overlap" terms in the evaluation of transition matrix elements. On including these overlap terms, differences between length- and velocity-form oscillator strengths were found to decrease systematically with increasing Z along the isoelectronic sequence. The relativistic random phase approximation (RRPA) was used by Lin and Johnson [32] to calculate oscillator strengths for the two lines $2s^2\,{}^1S_0$–$2s2p\,{}^1P_1$ and $2s^2\,{}^1S_0$–$2s2p\,{}^3P_1$. In the truncated relativistic RPA calculations [32], differences between length and velocity results are small in comparison with the differences obtained in MCDF calculations but remain significant for low-Z elements. Including the couplings with the $1s^2$ shell in the full RRPA, the length and velocity results agree to better than four figures. It was found in [32], that the velocity results for the oscillator strengths were altered substantially by including the coupling with the 1s shell, whereas the length results were modified only slightly. Extensive MCDF calculations were performed by Cheng, Kim and Desclaux [33] to obtain oscillator strengths and transition probabilities for the 16 possible E1 lines in the Be sequence for all ions with $Z \leqslant 30$ and for representative ions with $Z > 30$. Only configurations within the $n = 2$ complex were included to account for electron correlation and intermediate coupling. Results were presented in length form only. Accurate *ab initio* multi configuration Dirac–Fock (MCDF) calculations of lifetimes of the spin-forbidden $2s^2\,{}^1S_0$–$2s2p\,{}^3P_1$ transition and the spin-allowed $2s^2\,{}^1S_0$–$2s2p\,{}^1P_1$ transition in Be-like ions were performed by Ynnerman and Froese Fisher [34]. Contributions of valence–valence correlation, core-polarization and selected triples and quadruples were included in the calculations of Ref. [34], and the discrepancy between length and velocity forms for intercombination lines in the lighter ions were investigated. The A-value for the intercombination line in C III gave $100s^{-1}$ and $174s^{-1}$ in length and velocity forms, respectively. A similar discrepancy between length and velocity forms for the intercombination line in B II was

reported by Ynnerman and Froese Fisher [35], where the MCHF and MCDF methods were also compared.

In the present paper, we use relativistic many-body perturbation theory (MBPT) to determine reduced matrix elements, oscillator strengths and transition rates for all 16 allowed and forbidden electric dipole 2s–2p transitions in berylliumlike ions with nuclear charges ranging from $Z = 4$ to 100. We evaluate retarded E1 matrix elements in both length and velocity forms. Relativistic MBPT calculations starting from a local potential are gauge independent order-by-order, providing "derivative terms" are included in the second- and higher-order matrix elements and careful attention is paid to negative-energy states. The present MBPT calculations, however, start from a nonlocal $1s^2$ Dirac–Fock potential and consequently give gauge-dependent transition matrix elements. Indeed, our first-order matrix elements are identical to the MCDF matrix elements given in Refs. [29, 30, 33] and exhibit the gauge dependence characteristic of all such calculations. The second-order correlation corrections compensate almost exactly for the gauge dependence of the first-order matrix elements, leading to corrected matrix elements that differ by less than 1% in length and velocity forms throughout the periodic system. It should be emphasized that this close agreement is obtained only after virtual electron–positron pair contributions are included in the second-order elements. Our model space consists of all possible $n = 2$ configurations, leading to 4 odd-parity and 6 even-parity states. We use first-order perturbation theory to obtain intermediate coupling coefficients and second-order MBPT to determine matrix elements. The transition energies used in the evaluation of oscillator strengths and transition rates are obtained from a previous second-order MBPT calculation [38].

The present calculations lead to results for allowed transitions that are in excellent agreement with values from previous calculations throughout the isoelectronic sequence. There are substantial differences, however, between the present results and previous accurate calculations for forbidden transitions in the lightest few ions, owing in part to truncating the perturbation expansion at second order. These calculations are presented as a theoretical benchmark for comparison with experiment and theory. The results could be further improved by including third-order correlation corrections.

2. Method

In this section, we write down and discuss the relativistic MBPT formulas for first- and second-order transition matrix elements in atomic systems with two valence electrons. The formulas for first-order matrix elements are identical to those used in recent CI calculation [36] for He-like ions. The second-order matrix elements consists of Hartree–Fock (HF), random-phase approximation (RPA), correlation, and derivative terms. The HF and RPA contributions are identical to the corresponding terms for atoms with one valence electron given, for example, in [37]. The correlation term is a contribution involving both valence electrons and has no one-electron counterpart. We use the MBPT formalism developed in [38] to describe the perturbed wave functions, and to obtain the second-order energies used to evaluate oscillator strengths and transition rates; we list only those formulas which are needed to calculate reduced matrix elements in atomic systems with two electrons above a closed core.

2.1. *Basic formulas*

The first-order reduced dipole matrix element $Z^{(1)}$ for the transition between two states $vw(J)$–$v'w'(J')$ is [36]

$$Z^{(1)}[v_1w_1(J)\text{–}v_2w_2(J')] = \sqrt{[J][J']}\sum_{vw}\sum_{v'w'} \mathsf{S}^J(v_1w_1, vw)\,\mathsf{S}^{J'}(v_2w_2, v'w') \times (-1^{1+j_w+j_{v'}}\begin{Bmatrix} J & J' & 1 \\ j_{v'} & j_w & j_v \end{Bmatrix} Z_{v'w}\,\delta_{vw'}, \tag{1}$$

where $[J] = 2J + 1$. The quantity $\mathsf{S}^J(v_1w_1, vw)$ is a symmetry coefficient defined by

$$\mathsf{S}^J(v_1w_1, vw) = \eta_{v_1w_1}[\delta_{v_1v}\,\delta_{w_1w} + (-1)^{j_v+j_w+J+1}\delta_{v_1w}\,\delta_{w_1v}], \tag{2}$$

where η_{vw} is a normalization factor given by

$$\eta_{vw} = \begin{cases} 1 & \text{for } w \neq v, \\ 1/\sqrt{2} & \text{for } w = v. \end{cases}$$

The dipole matrix element Z_{vw}, which includes retardation, is given in velocity and length forms (see eqs 38, 39) of Ref. [36], $Z_{vw} = (3/k)\langle v\|t_1^{(1)}\|w\rangle$) by:

velocity form

$$Z_{vw} = \langle\kappa_v\|C_1\|\kappa_w\rangle\,\frac{3}{k}\int_0^\infty \mathrm{d}r\left\{\frac{j_1(kr)}{kr}\,[G_v(r)F_w(r) - F_v(r)G_w(r)] - \frac{\kappa_v - \kappa_w}{2}\left[2\,\frac{j_1(kr)}{kr} - j_2(kr)\right] \times [G_v(r)F_w(r) + F_v(r)G_w(r)]\right\} \tag{3}$$

length form

$$Z_{vw} = \langle\kappa_v\|C_1\|\kappa_w\rangle\,\frac{3}{k}\int_0^\infty \mathrm{d}r\left\{j_1(kr)[G_v(r)G_w(r) + F_v(r)F_w(r)] + j_2(kr)\left[\frac{\kappa_v - \kappa_w}{2}\,(G_v(r)F_w(r) + F_v(r)G_w(r)) + (G_v(r)F_w(r) - F_v(r)G_w(r))\right]\right\}. \tag{4}$$

Here κ_v is the angular momentum quantum number [$\kappa_v = \mp(j_v + \frac{1}{2})$ for $j_v = (l_v \pm \frac{1}{2})$] and $k = \alpha\omega$, where ω is the photon energy: $\omega = \varepsilon_w - \varepsilon_v$ for Z_{vw}. The quantity $C_{1q}(\hat{r})$ is a normalized spherical harmonic. The functions $G_a(r)$ and $F_a(r)$ are large- and small-component radial Dirac wave functions, respectively. The single-particle matrix elements $Z_{vw}(k)$ reduce to the velocity- and length-form matrix elements of the dipole operator in the limit $k \to 0$.

As mentioned previously, the second-order reduced matrix element $Z^{(2)}$ for the transition between the two states $vw(J)$–$v'w'(J')$ consists of four contributions: $Z^{(\mathrm{HF})}$, $Z^{(\mathrm{RPA})}$,

$Z^{(\mathrm{corr})}$, and $Z^{(\mathrm{derv})}$:

$$Z^{(\mathrm{HF})}[v_1w_1(J)\text{–}v_2w_2(J')] = \sqrt{[J][J']}\sum_{vw}\sum_{v'w'} \mathsf{S}^J(v_1w_1, vw)\mathsf{S}^{J'}(v_2w_2, v'w') \times (-1)^{1+j_w+j_{v'}}\begin{Bmatrix} J & J' & 1 \\ j_{v'} & j_w & j_v \end{Bmatrix} \times \sum_i \left[\frac{Z_{v'i}\Delta_{iw}}{\epsilon_i-\epsilon_w} + \frac{Z_{iw}\Delta_{v'i}}{\epsilon_i-\epsilon_{v'}}\right]\delta_{vw'} \tag{5}$$

$$Z^{(\mathrm{RPA})}[v_1w_1(J)\text{–}v_2w_2(J')] = \tfrac{1}{3}\sqrt{[J][J']}\sum_{vw}\sum_{v'w'} \mathsf{S}^J(v_1w_1, vw) \times \mathsf{S}^{J'}(v_2w_2, v'w')(-1)^{j_{w'}+j_v}\begin{Bmatrix} J & J' & 1 \\ j_{v'} & j_w & j_v \end{Bmatrix} \times \sum_n\sum_b \left[\frac{Z_{bn}Z_K(wbv'n)}{\epsilon_n+\epsilon_{v'}-\epsilon_w-\epsilon_b} + \frac{Z_{nb}Z_K(wnv'b)}{\epsilon_n+\epsilon_w-\epsilon_{v'}-\epsilon_b}\right]\delta_{vw'} \tag{6}$$

$$Z^{(\mathrm{corr})}[v_1w_1(J)\text{–}v_2w_2(J')] = \sqrt{[J][J']}\sum_{vw}\sum_{v'w'} \mathsf{S}^J(v_1w_1, vw)\mathsf{S}^{J'}(v_2w_2, v'w') \times \sum_k (-1)^{1+k}\sum_i \left[\frac{Z_{iv}X_k(v'w'wi)}{\epsilon_i+\epsilon_w-\epsilon_{v'}-\epsilon_{w'}} \times \begin{Bmatrix} J & J' & 1 \\ j_i & j_v & j_w \end{Bmatrix}\begin{Bmatrix} j_i & j_w & J' \\ j_{v'} & j_{w'} & k \end{Bmatrix}(-1)^{J+j_w+j_{w'}} + \frac{Z_{v'i}X_k(iw'vw)}{\epsilon_i+\epsilon_{w'}-\epsilon_v-\epsilon_w}\begin{Bmatrix} J' & J & 1 \\ j_i & j_{v'} & j_{w'} \end{Bmatrix} \times \begin{Bmatrix} j_i & j_{w'} & J \\ j_w & j_v & k \end{Bmatrix}(-1)^{j_v+j_{v'}}\right]. \tag{7}$$

In the above equations, the index b designates core states, n designates excited states, and i denotes an arbitrary core or excited state. In the sums over i in eq. (5), all terms with vanishing denominators are excluded. In the sum occurring in the first term of eq. (7), states i for which (iw) is in the model space of final states $(v'w')$ are excluded, while in the second term, states i for which (iw') is in the model space of initial states (vw) are excluded. In the sums over n in the RPA matrix elements (6), all core states are excluded. The definitions of $X_k(abcd)$ and $Z_k(abcd)$ are given by eq. (2.12) and eq. (2.15) in Ref. [38] and Δ_{ij} is defined at the end of Section II in [38]. The second-order reduced matrix element of the derivative term is given by:

$$Z^{(\mathrm{derv})}[vw(J)\text{–}v'w'(J')] = \alpha(E^{(1)}_{vw} - E^{(1)}_{v'w'})P^{(\mathrm{derv})}[vw(J)\text{–}v'w'(J')] \tag{8}$$

where $E^{(1)}_{vw}$, is the first-order correction to the energy defined by eqs. (2.8–2.10) in Ref. [38] and the quantity $P^{(\mathrm{derv})}$ is defined by

$$P^{(\mathrm{derv})}[v_1w_1(J)\text{–}v_2w_2(J')] = \sqrt{[J][J']}\sum_{vw}\sum_{v'w'} \mathsf{S}^J(v_1w_1, vw)\mathsf{S}^{J'}(v_2w_2, v'w') \times (-1)^{1+j_w+j_{v'}}\begin{Bmatrix} J & J' & 1 \\ j_{v'} & j_w & j_v \end{Bmatrix} Z^{(\mathrm{derv})}_{v'w}\delta_{vw'}. \tag{9}$$

The expression for $Z^{(\mathrm{derv})}_{vw}$ is obtained from $\omega\langle v\|(\mathrm{d}t^{(1)}_1/\mathrm{d}\omega)\|w\rangle$. The following formulas give the velocity and length forms for this quantity:

velocity form

$$Z^{(\mathrm{derv})}_{vw} = \langle\kappa_v\|C_1\|\kappa_w\rangle\frac{3}{k}\int_0^\infty \mathrm{d}r\Big\{-j_2(kr) \times [G_v(r)F_w(r) - F_v(r)G_w(r)] - \frac{\kappa_v-\kappa_w}{2}[j_2(kr) - (kr)j_1(kr)] \times [G_v(r)F_w(r) + F_v(r)G_w(r)]\Big\}, \tag{10}$$

length form

$$Z^{(\mathrm{derv})}_{vw} = \langle\kappa_v\|C_1\|\kappa_w\rangle\frac{3}{k}\int_0^\infty \mathrm{d}r\Big\{[j_1(kr) - (kr)j_2(kr)] \times [G_v(r)G_w(r) + F_v(r)F_w(r)] + \Big[-3j_2(kr) + (kr)j_1(kr)\Big] \times \Big[\frac{\kappa_v-\kappa_w}{2}(G_v(r)F_w(r) + F_v(r)G_w(r)) + [G_v(r)F_w(r) - F_v(r)G_w(r)]\Big]\Big\} \tag{11}$$

All of the second-order correlation corrections above are from the residual Coulomb interaction. To include correlation corrections from the Breit interaction, the Coulomb matrix element $X_k(abcd)$ must be modified according to the rule:

$$X_k(abcd) \to X_k(abcd) + M_k(abcd) + N_k(abcd). \tag{12}$$

The magnetic radial integrals M_k and N_k are defined by eqs (A4, A5) in Ref. [39].

2.2. *Uncoupled matrix elements*

In Table I, we list values of $Z^{(1)}$, $Z^{(\mathrm{RPA})}$, $Z^{(\mathrm{corr})}$, and $P^{(\mathrm{derv})}$ for $J = 0 - J' = 1$ transitions in Be-like iron, $Z = 26$. Both length and velocity forms of the matrix elements are given. In the table, we use the label B to denote the Breit contributions and we tabulate $1000 \times B^{(\mathrm{HF})}$, $1000 \times B^{(\mathrm{RPA})}$, $1000 \times B^{(\mathrm{corr})}$, together with the sum, $1000 \times B^{(2)}$. It can be seen from Table I that even the first-order contributions $Z^{(1)}$ are different in length and velocity forms. It is also apparent that the Breit corrections $B^{(2)}$ are 3–6 times smaller than $Z^{(\mathrm{RPA})}$, and that the RPA terms are 3–6 times smaller than $Z^{(\mathrm{corr})}$. These ratios change with nuclear charge owing to the Z-dependence of the various terms:

$$Z^{(1)} = \frac{1}{Z}[p_{10} + p_{12}(\alpha Z)^2 + p_{14}(\alpha Z)^4 + \cdots] + \frac{1}{Z^2}[p^{\mathrm{HF}}_{20} + p^{\mathrm{HF}}_{22}(\alpha Z)^2 + p^{\mathrm{HF}}_{24}(\alpha Z)^4 + \cdots] + \cdots, \tag{13}$$

$$Z^{(\mathrm{RPA})} + Z^{(\mathrm{corr})} = \frac{1}{Z^2}\Big[p^{\mathrm{corr}}_{20} + p^{\mathrm{corr}}_{22}(\alpha Z)^2 + p^{\mathrm{corr}}_{14}(\alpha Z)^4 + \cdots] + \frac{1}{Z^3}[p^{\mathrm{HF}}_{30} + p^{\mathrm{HF}}_{32}(\alpha Z)^2 + p^{\mathrm{HF}}_{34}(\alpha Z)^4 + \cdots] + \cdots, \tag{14}$$

Table I. *Uncoupled reduced matrix elements in length (L) and velocity (V) forms for Fe^{+22}. Notation:* $2p = 2p_{3/2}$, $2p^* = 2p_{1/2}$

(a) Coulomb Interaction:

$vw(J]$	$v'w'[J']$		$Z^{(1)}$	$P^{(\mathrm{derv})}$	$Z^{(\mathrm{RPA})}$	$Z^{(\mathrm{corr})}$
2s2s[0]	2s2p*[1]	(L)	0.172 296	0.172 301	−0.000 349	0.002 141
		(V)	0.188 645	0.000 011	−0.016 192	0.028 821
2s2s[0]	2s2p[1]	(L)	−0.245 591	−0.245 577	−0.000 489	−0.003 047
		(V)	−0.262 761	0.000 026	0.017 130	−0.028 097
2p*2p*[0]	2s2p*[1]	(L)	−0.172 296	−0.172 301	0.000 350	−0.000 141
		(V)	−0.188 645	−0.000 011	0.016 192	−0.137 875
2p*2p*[0]	2s2p[1]	(L)	0.000 000	0.000 000	0.000 000	−0.001 803
		(V)	0.000 000	0.000 000	0.000 000	0.138 604
2p2p[0]	2s2p*[1]	(L)	0.000 000	0.000 000	0.000 000	0.001 760
		(V)	0.000 000	0.000 000	0.000 000	−0.052 784
2p2p[0]	2s2p[1]	(L)	0.173 659	0.173 649	−0.000 345	−0.001 187
		(V)	0.185 800	−0.000 019	−0.012 113	0.149 421

(b) Breit Interaction with factor 10^3:

$vw[J]$	$v'w'[J']$		$B^{(\mathrm{HF})}$	$B^{(\mathrm{RPA})}$	$B^{(\mathrm{corr})}$	$B^{(2)}$
2s2s[0]	2s2p*[1]	(L)	0.098 080	−0.004 836	0.004 279	0.097 522
		(V)	1.099 649	0.907 263	−0.515 062	1.491 849
2s2s[0]	2s2p[1]	(L)	−0.067 346	0.000 852	−0.013 697	−0.080 190
		(V)	0.618 200	−0.526 286	0.356 316	0.448 230
2p*2p*[0]	2s2p*[1]	(L)	−0.098 080	0.004 836	0.000 408	−0.092 836
		(V)	−1.099 649	−0.907 263	−1.066 757	−3.073 668
2p*2p*[0]	2s2p[1]	(L)	0.000 000	0.000 000	−0.000 115	−0.001 153
		(V)	0.000 000	0.000 000	1.036 049	1.036 049
2p2p[0]	2s2p*[1]	(L)	0.000 000	0.000 000	−0.000 405	−0.004 047
		(V)	0.000 000	0.000 000	−0.575 952	−0.575 952
2p2p[0]	2s2p[1]	(L)	0.047 621	−0.000 603	0.018 465	0.065 483
		(V)	−0.437 133	0.372 140	1.570 535	1.505 543

$$B^{(2)} = \frac{1}{Z^2}(\alpha Z)^2[b_{10} + b_{12}(\alpha Z)^2 + b_{14}(\alpha Z)^4 + \cdots] + \frac{1}{Z^3}(\alpha Z)^2[b_{20}^{\mathrm{HF}} + b_{22}^{\mathrm{HF}}(\alpha Z)^2 + b_{24}^{\mathrm{HF}}(\alpha Z)^4 + \cdots] + \cdots. \tag{15}$$

We find, for example, that the first-order contribution $Z^{(1)}$ for the $2s2p_{1/2}(0)$–$2p_{1/2}2p_{3/2}(1)$ transition decreases by a factor of 6 from $Z = 4$ to $Z = 16$, and by a factor 8 from $Z = 16$ to $Z = 100$ (see eq. (13)). The second-order contribution $Z^{(\mathrm{RPA})} + Z^{(\mathrm{corr})}$ decreases more rapidly with Z as can be seen by comparing eq. (13) with eq. (14). The value of this contribution for $2s2p_{1/2}(0)$–$2p_{1/2}2p_{3/2}(1)$ transition decreases by a factor of 35 from $Z = 4$ to $Z = 16$ and by a factor of 24 from $Z = 16$ to $Z = 100$. The situation is completely different for the Breit contribution as can be seen in eq (15); we find that the contribution $B^{(2)}$ for the $2s2p_{1/2}(0)$–$2p_{1/2}2p_{3/2}(1)$ transition increases by 36% from $Z = 4$ to $Z = 16$ then decreases by 3% from $Z = 16$ to $Z = 100$.

2.3. *Coupled matrix elements*

The physical two-particle states are linear combinations of uncoupled two-particle states (vw) in the model space having fixed values of angular momentum and parity; consequently, the transition amplitudes between physical states are linear combinations of the uncoupled transition matrix elements given in Table I. The expansion coefficients and energies are obtained by diagonalizing the effective Hamiltonian as discussed in [38]. The first-order expansion coefficient $C_1^{\lambda}(vw)$ is the λ-th eigenvector of the first-order effective Hamiltonian, and E_1^{λ} is the corresponding eigenvalue. In the present calculation, both Coulomb and Breit interactions are included in the first-order effective Hamiltonian. The coupled transition matrix element between the I-th, initial eigenstate which has angular momentum J and the F-th final state which has angular momentum J' is given by

$$\begin{aligned} Q^{(1+2)}(I-F) = \frac{1}{E_1^I - E_1^F} \sum_{vw} \sum_{v'w'} & C_1^I(vw) C_1^F(v'w') \\ & \times \{[\epsilon_{vw} - \epsilon_{v'w'}][Z^{(1+2)}[vw(J)\text{–}v'w'(J')] \\ & \qquad + B^{(2)}[vw(J)\text{–}v'w'(J')]] \\ & + [E_1^I - E_1^F - \epsilon_{vw} + \epsilon_{v'w'}] \\ & \times P^{(\mathrm{derv})}[vw(J)\text{–}v'w'(J')]\}. \end{aligned} \tag{16}$$

Here $\epsilon_{vw} = \epsilon_v + \epsilon_w$ and $Z^{(1+2)} = Z^{(1)} + Z^{(\mathrm{RPA})} + Z^{(\mathrm{corr})}$. Using these formulas and the results for uncoupled reduced matrix elements given in Table I, we transform from uncoupled reduced matrix elements to intermediate coupled reduced matrix elements between physical states.

In Table II, we present values of the sixteen $2l_1 2l_2[LSJ]$–$2l_3 2l_4[L'S'J']$ coupled reduced matrix elements in length (L) and velocity (V) forms for Be-like iron, $Z = 26$. Although we use an intermediate-coupling scheme, it is nevertheless convenient to label the physical states using the $[LSJ]$ designation. We can see that the results obtained in the two forms (L) and (V) differ only in fourth digit except for two transitions $2s2p\,^3P_1$–$2p^2\,^1S_0$ and $2s2p\,^3P_1$–$2p^2\,^1D_2$. These disagreements in the third or fourth digits arise because we use a non-local Hartree–Fock potential. It was already shown by Johnson, Plante and Sapirstein [36] that for He-like ions gauge-independent first-order and second-order reduced matrix elements can be obtained using a local Hartree or

Table II. *Coupled reduced matrix elements Q calculated in length- and velocity-forms for Fe^{+22}. Velocity-form matrix elements are given with (a) and without (b) negative-energy contributions*

$l_1 l_2\, LSJ$	$l'_1 l'_2\, L'S'J'$	length	velocity[a]	velocity[b]
$2s^2\,{}^1S_0$	$2s2p\,{}^1P_1$	0.256 978	0.257 267	0.256 155
$2s^2\,{}^1S_0$	$2s2p\,{}^3P_1$	0.034 580	0.034 611	0.035 404
$2s2p\,{}^1P_1$	$2p^2\,{}^3P_0$	0.034 859	0.034 812	0.035 684
$2s2p\,{}^3P_1$	$2p^2\,{}^3P_0$	0.175 435	0.175 672	0.175 257
$2s2p\,{}^1P_1$	$2p^2\,{}^1S_0$	0.224 878	0.225 035	0.224 281
$2s2p\,{}^3P_1$	$2p^2\,{}^1S_0$	0.008 729	0.008 752	0.008 622
$2s2p\,{}^3P_0$	$2p^2\,{}^3P_1$	0.174 519	0.174 739	0.173 824
$2s2p\,{}^1P_1$	$2p^2\,{}^3P_1$	0.022 462	0.022 490	0.023 002
$2s2p\,{}^3P_1$	$2p^2\,{}^3P_1$	0.149 050	0.149 238	0.148 585
$2s2p\,{}^3P_2$	$2p^2\,{}^3P_1$	0.193 450	0.193 727	0.193 452
$2s2p\,{}^1P_1$	$2p^2\,{}^3P_2$	0.159 464	0.159 241	0.159 190
$2s2p\,{}^3P_1$	$2p^2\,{}^3P_2$	0.197 836	0.198 054	0.196 759
$2s2p\,{}^1P_1$	$2p^2\,{}^1D_2$	0.347 082	0.346 968	0.345 137
$2s2p\,{}^3P_1$	$2p^2\,{}^1D_2$	0.042 156	0.042 259	0.042 163
$2s2p\,{}^3P_2$	$2p^2\,{}^3P_2$	0.293 314	0.293 720	0.292 798
$2s2p\,{}^3P_2$	$2p^2\,{}^1D_2$	0.165 847	0.166 061	0.164 952

Coulomb potential. The arguments of that paper are easily extended to Be-like ions.

Let us confirm this conclusion for the transition $2s2p\,{}^3P_0$–$(2p)^2\,{}^3P_1$. For this example, both initial and final states are single-configuration states in any coupling scheme. In Table III, we present a breakdown of the contributions for this transition in Be-like iron. In the first two columns, we compare results obtained with a (local) Coulomb potential in L and V forms. We see that the first-order results and second-order results are identical in the two forms to the 6 digits quoted. (This is true independently for the Coulomb and Breit interactions.) We do not obtain precise agreement between L and V forms for the nonlocal HF potential given in the last two columns of the table. However, the differences between L- and V-forms of the matrix element, which range between 0.1% and 1% for the transitions shown in Table I, are smaller the uncertainties in available experimental data.

2.4. *Virtual electron–positron pair contributions*

In this subsection, we examine the effect of electron–positron pair contributions to the second-order reduced matrix element. These contributions arise from the terms in the sum over states i and n in eqs (5–7) for which $\varepsilon_i < -mc^2$. The contribution of the negative-energy terms was discussed by Johnson, Plante and Sapirstein [36] for He-like ions, where it was shown that they are most important for velocity-form matrix elements and do not significantly modify length-form matrix elements; we confirm that this conclusion is valid for Be-like ions also. In the final column of Table III, we list the velocity-form of the coupled reduced matrix elements calculated without negative-energy components. Comparison of results for the velocity-form matrix element, calculated (a) with and (b) without negative-energy components shows the large contribution (10–30%) for transitions with $\Delta S = 1$. The negative-energy contributions from the sum over states leads to very small changes in the length-form matrix elements but substantial changes in some of the velocity-form matrix elements, leading to gauge independence.

Table III. *Breakdown of the coupled reduced matrix element in length (L) and velocity (V) forms for the* $2s2p\,{}^3P_0$–$(2p)^2\,{}^3P_1$ *transition in* Fe^{+22}

	(a) Coulomb potential		(b) Dirac–Fock potential	
	L	V	L	V
$Z^{(1)}$	0.162 181 8	0.162 181 8	0.173 659	0.185 800
$Z^{(\mathrm{derv})}$	0.529 166 9	−0.000 018 3	0.053 120	−0.000 006
$Z^{(2)}$	0.011 593 7	0.540 778 9	0.001 071	0.042 302
$B^{(\mathrm{derv})}$	0.000 613 3	0.000 000 0	0.000 109	0.000 000
$B^{(2)}$	0.000 055 5	0.000 668 8	0.000 056	0.000 205
$(Z+B)^{(\mathrm{tot})}$	0.703 611 2	0.703 611 2	0.228 015	0.228 301
Q	0.164 909 9	0.164 909 9	0.174 519	0.174 738

3. Results and discussion

We calculate line strengths, oscillator strengths and transition probabilities for sixteen $2l_1 2l_2[LSJ]$–$2l_3 2l_4[L'S'J']$ lines for all ions up to $Z = 30$, and for representative high-Z ions with $Z = 32$, 36, 40, 42, 50, 54, 60, 63, 70, 74, 79, 80, 83, 90, 92, 100. The results were obtained in both length and velocity forms but only length-form results are tabulated. The theoretical energies used to evaluate oscillator strengths and transition probabilities are taken from Ref. [38].

In Fig. 1, we illustrate the Z-dependence of the differences between line strengths calculated in length $S(L)$ and velocity $S(V)$ forms. We plot the ratio $(S(L) - S(V))/S(L)$ in percent. We separately show LS-allowed transitions in Fig. 1a and LS-forbidden transitions in Fig. 1b. One can see that the agreement between length and velocity forms improves with increasing Z. The ratio $(S(L) - S(V))/S(L)$ is about 0.1–0.2% starting from $Z = 30$ for all transitions except $2s2p\,{}^3P_1$–$2p^2\,{}^1S_0$. It should be noted that the line strengths for this transition become very small (10^{-9}) for $Z > 50$, which is a factor of 10^6–10^4 less than all other transitions. The largest values for the ratio are for $Z = 4$ and 5 where the ratio is 0.5–1% for allowed transitions and 10–100% for forbidden transitions. Two peaks are evident in Fig. 1b for the $(S(L) - S(V))/S(L)$ ratio of $2s2p\,{}^1P_1$–$2p^2\,{}^3P_0$ transitions. These peaks are explained by reversing the $2s2p\,{}^1P_1$ and $2p^2\,{}^3P_0$ levels, as we will explain later.

In Fig. 2 we present the Z-dependence of the difference between velocity-form line strengths Sn, calculated with both positive- and negative-energy contributions, and Sp, calculated with positive-energy components only. We plot the ratio $(Sn - Sp)/Sn$ in percent. The 16 transitions are again divided into LS-allowed transitions shown in Fig. 2a and LS-forbidden transitions shown in Fig. 2b. Comparing Fig. 2a with Fig. 1a, one sees that the values of $(Sn - Sp)/Sn$ are larger than the values of $(S(L) - S(V))/S(L)$ by a factor of 10 or more for $Z > 20$. The contributions of the negative-energy components are much larger for transition as seen in Fig. 2b, especially for small Z. The velocity-form line strength for the $2s^2\,{}^1S_0$–$2s2p\,{}^1P_1$ transition changes by a factor of 30 for $Z = 5$ and in by a factor of 2 for $Z = 6$. These changes can be understood by the very large negative-energy contributions to the Breit terms $B^{(\mathrm{HF})}$, $B^{(\mathrm{RPA})}$, and $B^{(\mathrm{corr})}$. The values of these terms change by a factor of two when the negative-energy components are included. This influence of negative-energy components gives us a key to understanding the large disagreement

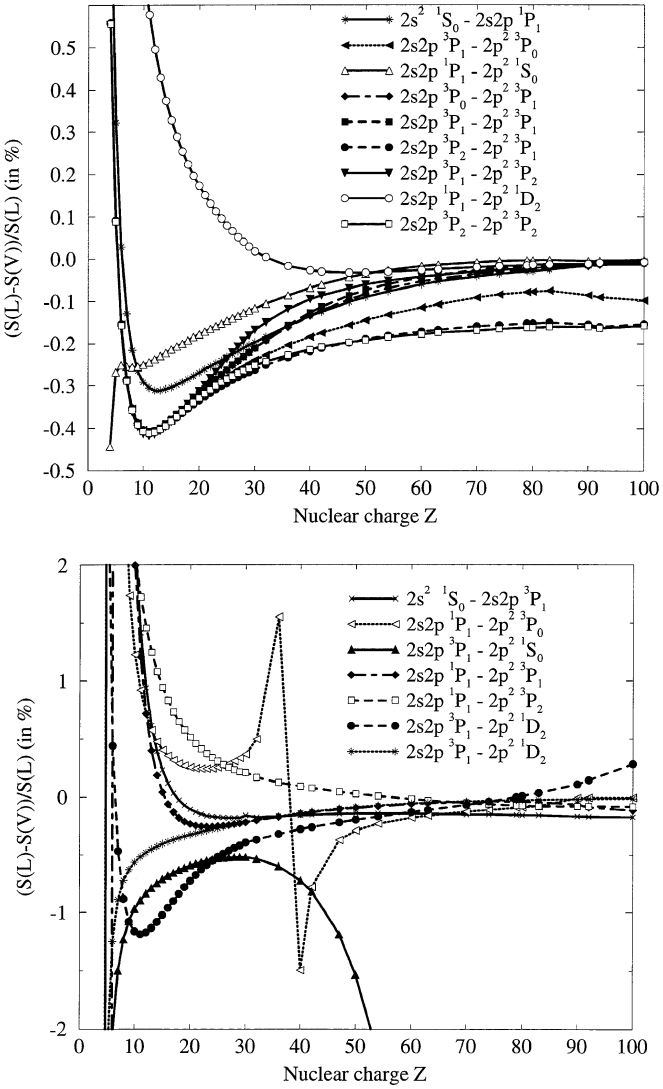

Fig. 1. Z-dependence of the ratio $(S(L) - S(V)/S(L)$ in %, where line strengths S are calculated in length $S(L)$ and velocity $S(V)$ forms. (a)-allowed transitions, (b) forbidden in LS-coupling scheme transitions.

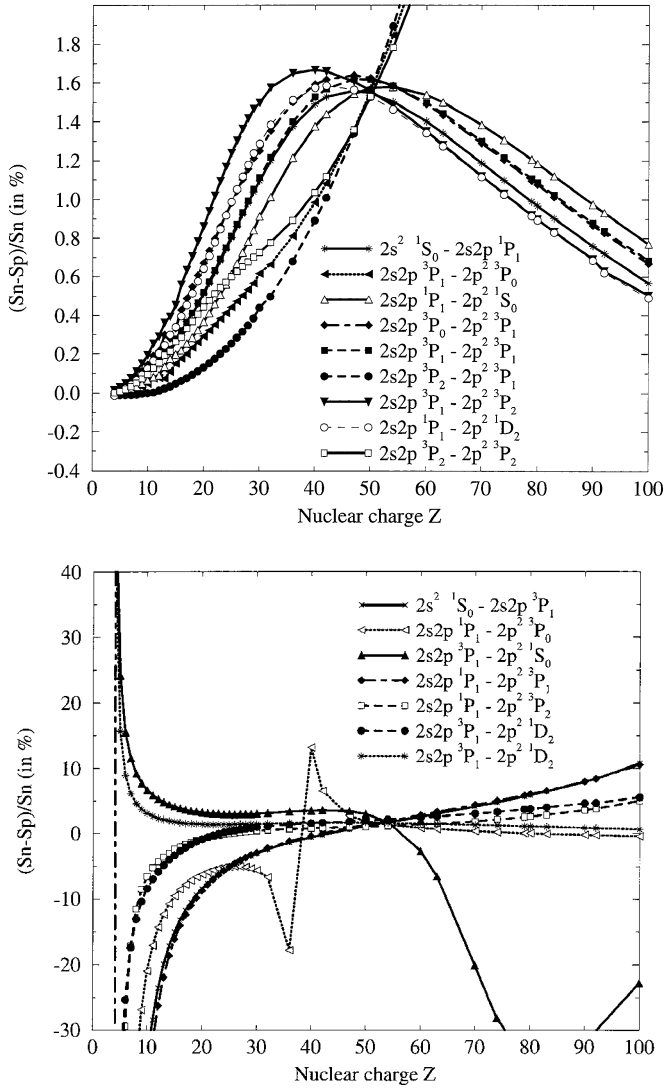

Fig. 2. Z-dependence of the ratio $(Sn - Sp)/Sn$ in %, where S-values are calculated in velocity form, with-Sn and without-Sp negative-energy components. (a)-allowed transitions, (b) forbidden in LS-coupling scheme transitions.

between length- and velocity-form line strengths obtained using MCDF found in [30, 31, 34, 35].

In Table IV, we list the values of line strengths S, calculated in length form. These values are given for $Z = 4$, 10, 20, 40, 60, 80, and 100. We can see from this table, that the three LS forbidden transitions $2s2p\,^1P_1$–$2p^2\,^3P_0$, $2s2p\,^3P_1$–$2p^2\,^1S_0$, and $2s2p\,^3P_1$–$2p^2\,^1D_2$ are also forbidden transitions in jj coupling. The reduced dipole matrix elements Q for these three transitions vanish when the electron–electron interaction is omitted. We can see that the

Table IV. *Line strengths S in (au) as functions of Z*

[LS designation]		$Z = 10$	$Z = 20$	$Z = 40$	$Z = 60$	$Z = 80$	$Z = 100$	[jj designation]	
$2s^2\,^1S_0$	$-2s2p\,^1P_1$	5.51 (−1)	1.15 (−1)	2.54 (−2)	1.00 (−2)	5.11 (−3)	2.88 (−3)	2s2s [0]	$-2s2p_{3/2}$ [1]
$2s^2\,^1S_0$	$-2s2p\,^3P_1$	1.14 (−5)	4.12 (−4)	3.12 (−3)	2.52 (−3)	1.48 (−3)	7.99 (−4)	2s2s [0]	$-2s2p_{1/2}$ [1]
$2s2p\,^1P_1$	$-2p^2\,^3P_0$	2.62 (−5)	6.16 (−4)	8.72 (−4)	2.36 (−4)	7.97 (−5)	3.37 (−5)	$2s2p_{3/2}$ [1]	$-2p_{1/2}2p_{1/2}$ [0]
$2s2p\,^3P_1$	$-2p^2\,^3P_0$	2.68 (−1)	5.40 (−2)	1.31 (−2)	5.50 (−3)	2.61 (−3)	1.28 (−3)	$2s2p_{1/2}$ [1]	$-2p_{1/2}2p_{1/2}$ [0]
$2s2p\,^1P_1$	$-2p^2\,^1S_0$	4.90 (−1)	9.56 (−2)	1.63 (−2)	5.62 (−3)	2.71 (−3)	1.49 (−3)	$2s2p_{3/2}$ [1]	$-2p_{3/2}2p_{3/2}$ [0]
$2s2p\,^3P_1$	$-2p^2\,^1S_0$	2.75 (−6)	4.92 (−5)	1.15 (−5)	5.78 (−8)	1.82 (−9)	1.14 (−9)	$2s2p_{1/2}$ [1]	$-2p_{3/2}2p_{3/2}$ [0]
$2s2p\,^3P_0$	$-2p^2\,^3P_1$	2.69 (−1)	5.41 (−2)	1.20 (−2)	4.98 (−3)	2.57 (−3)	1.45 (−3)	$2s2p_{1/2}$ [0]	$-2p_{1/2}2p_{3/2}$ [1]
$2s2p\,^1P_1$	$-2p^2\,^3P_1$	5.39 (−6)	1.83 (−4)	1.19 (−3)	8.78 (−4)	4.83 (−4)	2.52 (−4)	$2s2p_{3/2}$ [1]	$-2p_{1/2}2p_{3/2}$ [1]
$2s2p\,^3P_1$	$-2p^2\,^3P_1$	2.01 (−1)	4.03 (−2)	7.71 (−3)	2.74 (−3)	1.34 (−3)	7.40 (−4)	$2s2p_{1/2}$ [1]	$-2p_{1/2}2p_{3/2}$ [1]
$2s2p\,^3P_2$	$-2p^2\,^3P_1$	3.35 (−1)	6.70 (−2)	1.44 (−2)	5.64 (−3)	2.68 (−3)	1.33 (−3)	$2s2p_{3/2}$ [2]	$-2p_{1/2}2p_{3/2}$ [1]
$2s2p\,^1P_1$	$-2p^2\,^3P_2$	2.92 (−4)	1.03 (−2)	1.84 (−2)	6.37 (−3)	2.83 (−3)	1.37 (−3)	$2s2p_{3/2}$ [1]	$-2p_{1/2}2p_{3/2}$ [2]
$2s2p\,^3P_1$	$-2p^2\,^3P_2$	3.36 (−1)	6.82 (−2)	2.08 (−2)	1.11 (−2)	6.16 (−3)	3.56 (−3)	$2s2p_{1/2}$ [1]	$-2p_{1/2}2p_{3/2}$ [2]
$2s2p\,^1P_1$	$-2p^2\,^1D_2$	1.25 (0)	2.51 (−1)	3.39 (−2)	1.28 (−2)	6.47 (−3)	3.61 (−3)	$2s2p_{3/2}$ [1]	$-2p_{3/2}2p_{3/2}$ [2]
$2s2p\,^3P_1$	$-2p^2\,^1D_2$	1.43 (−5)	6.42 (−4)	5.74 (−4)	3.17 (−5)	2.96 (−6)	4.26 (−7)	$2s2p_{1/2}$ [1]	$-2p_{3/2}2p_{3/2}$ [2]
$2s2p\,^3P_2$	$-2p^2\,^3P_2$	1.01 (0)	1.91 (−1)	1.93 (−2)	6.13 (−3)	2.77 (−3)	1.36 (−3)	$2s2p_{3/2}$ [2]	$-2p_{1/2}2p_{3/2}$ [2]
$2s2p\,^3P_2$	$-2p^2\,^1D_2$	3.54 (−4)	1.13 (−2)	2.52 (−2)	1.19 (−2)	6.33 (−3)	3.60 (−3)	$2s2p_{3/2}$ [2]	$-2p_{3/2}2p_{3/2}$ [2]

line strengths for these three transitions $2s^2\,^1S_0$–$2s2p\,^3P_1$, $2s2p\,^1P_1$–$2p^2\,^3P_1$, $2s2p\,^1P_1$–$2p^2\,^3P_2$, and $2s2p\,^3P_2$–$2p^2\,^1D_2$ are allowed transitions in the *jj* scheme. The line strengths for these transitions become comparable to those for *LS*-allowed transitions for $Z \geqslant 36$.

In Table V, we compare our results for the lifetimes of upper levels in Fe^{+22} with the experimental results of Bauchet *et al.* [40]. We also present wavelengths for one of the transitions which contribute in the lifetime of the upper level. For example, there are three radiative channels for the E1 decay of the $2p^2\,^3P_2$ state: $2p^2\,^3P_2 \rightarrow 2s2p\,^3P_2$, $2p^2\,^3P_2 \rightarrow 2s2p\,^3P_1$, $2p^2\,^3P_2 \rightarrow 2s2p\,^1P_1$. There is good agreement between theoretical and experimental lifetimes. Lifetimes of three levels that were not measured in [40]: $2p^2\,^3P_0$, $2p^2\,^3P_1$, and $2s2p\,^3P_1$ are also given in the table.

In Table VI, we present the transition probabilities A for three lines: $2s^2\,^1S_0$–$2s2p\,^1P_1$, $2s2p\,^1P_1$–$2p^2\,^1S_0$, and $2s2p\,^1P_1$–$2p^2\,^1D_2$ for all ions up to $Z = 30$, and for representative high-Z ions. The A-values for these three LS-allowed transitions are given in the length form. We compare our theoretical results with available experimental data [40–50]. The experimental A-values for the $2s^2\,^1S_0$–$2s2p\,^{1,3}P_1$ resonance and intercombination lines were critically selected by Curtis and Ellis [41], and we use their data for comparison with our calculations. We take the experimental A-values for the other two lines from papers published in the 26 year interval 1969–1995. These experimental results included ions with $Z \leqslant 17$ and three high-Z ions with $Z = 26$, 36, and 54. We find good agreement between the theoretical and experimental results except for some low-Z data. It should be noted that the theoretical A-values for the $2s^2\,^1S_0$–$2s2p\,^1P_1$ line would increase by 37% for $Z = 4$, 15% for $Z = 5$, 8% for $Z = 6$, and 5% for $Z = 7$ if the theoretical energies were replaced by experimental ones. The recalculated values are given in Table VII. In this table, we compared our results with recent theoretical calculations given by Fleming *et al.* [19]. In this paper extensive configuration–interaction calculations was performed to obtain oscillator strengths for only one line $2s^2\,^1S_0$–$2s2p\,^1P_1$ for seven ions.

In Table VIII, we compare our results for the lifetimes of $2p^2[\,^3P_0,\ ^3P_1,\ ^3P_2]$ upper levels of ions $Z \leqslant 17$ with experimental results from [44–47, 50, 52–54]. The A-values for the six *LS* allowed transitions $2s2p\,^3P_1$–$2p^2\,^3P_0$, $2s2p\,^3P_0$–$2p^2\,^3P_1$, $2s2p\,^3P_1$–$2p^2\,^3P_1$, $2s2p\,^3P_2$–$2p^2\,^3P_1$, $2s2p\,^3P_1$–$2p^2\,^3P_2$, and $2s2p\,^3P_2$–$2p^2\,^3P_2$ are used to calculate the lifetimes of $2p^2\,^3P_0$, $2p^2\,^3P_1$, and $2p^2\,^3P_2$ levels. There is no large difference in A-values for different J in the interval $Z \leqslant 17$ so we did not specify J for the experimental lifetimes. Our theoretical A-values agree with experimental results for B^+ [47], C^{2+} [52], Si^{10+} [46], P^{11+} [44], and Cl^{13+} [50] but disagree for O^{4+} [54], and F^{5+} [45]. No error estimates were given for N^{3+} [53]. Our results are obtained using a single method for all Z and are expected to improve in accuracy for high Z. As a result, the agreement between theoretical and experimental data for small Z ($Z = 5$ and 6) allows us to infer that results for high Z are also reliable. We also obtain agreement between theoretical and experimental data for $Z = 14$, 15, 17. We conclude that experimental data for N^{3+} [53], O^{4+} [54], and F^{5+} [45] are not accurate.

The Z-dependence of oscillator strengths for the six triplet–triplet transitions $2s2p\,^3P_1$–$2p^2\,^3P_0$, $2s2p\,^3P_0$–$2p^2\,^3P_1$, $2s2p\,^3P_1$–$2p^2\,^3P_1$, $2s2p\,^3P_2$–$2p^2\,^3P_1$, $2s2p\,^3P_1$–$2p^2\,^3P_2$, and $2s2p\,^3P_2$–$2p^2\,^3P_2$ are illustrated on Fig. 3. Systematics of atomic oscillator strengths were investigated very early [20, 55, 56]. Such studies are useful for judging the reliability and accuracy of experimental data [57, 58, 41]. The present work demonstrates that oscillator strengths decrease as $1/Z$ for allowed 2s–2p transitions for ions with $Z < 36$. We can see from eqs (13–15) that the Z-dependence of the reduced matrix element $Q^{(1+2)}$ are rather complicated and include terms proportional to $1/Z$ and $(\alpha Z)^2$. Consequently, the reduced matrix elements $Q^{(1+2)}$ decrease more rapidly with Z than $1/Z$: by a factor of 14 from $Z = 4$ to $Z = 32$ then increases by a factor of 4 from $Z = 32$ to $Z = 100$ for $2s2p\,^3P_0$–$2p^2\,^3P_1$ transitions. It should be noted that both initial and final states of this transition are single configuration states so there is no influence of intermediate coupling coefficients for this matrix element. The same situation is also true for the $2s2p\,^3P_2$–$2p^2\,^3P_1$ transition where the oscillator strength decreases by a factor of 16 from $Z = 4$ to $Z = 32$ and by a factor of 4 from $Z = 32$ to $Z = 100$. The behavior of f-values for these two transitions is completely different for $Z > 32$ as shown in Fig. 3. This difference is explained by different behavior of transition energies for the two transitions. The Z-dependence of the energy in Be-like ions was investigated in [32] as shown in Fig. 3. This difference is explained by

Table V. *Wavelengths and lifetimes for upper level for Fe^{+22}. Experimental values are from* [40]

	λ in Å		τ in ps	
Transition	Theory	Expt.	Theory	Expt.
$2s2p\,^3P_2$–$2p^2\,^3P_2$	166.76	167	76.2	79 ± 8
$2s2p\,^1P_1$–$2p^2\,^1S_0$	149.28	149	32.3	34 ± 5
$2s2p\,^1P_1$–$2p^2\,^1D_2$	221.32	221	108	100 ± 8
$2s^2\,^1S_0$–$2s2p\,^1P_1$	132.98	133	52.7	51 ± 5
$2s^2\,^1S_0$–$2s2p\,^3P_1$	263.78		22730	
$2s2p\,^3P_1$–$2p^2\,^3P_0$	173.35		83.4	
$2s2p\,^3P_0$–$2p^2\,^3P_1$	147.34		67.4	

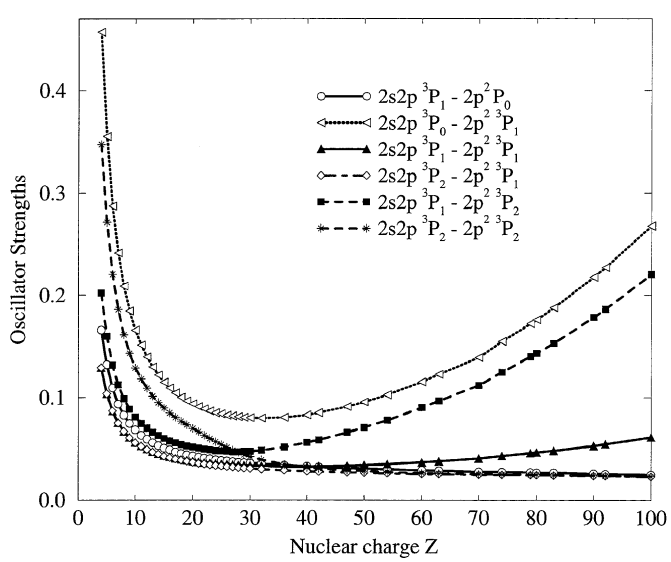

Fig. 3. Oscillator strengths of six *LS*-allowed $2s2p\,^3P_J$–$2p^2\,^3P_{J'}$ lines as functions of Z.

Table VI. *Transition probabilities (A in sec^{-1}) calculated in length (A_L) and velocity (A_V) forms, compared with experimental results for* $2s^2\,{}^1S_0$–$2s2p\,{}^1P_1$, $2s2p\,{}^1P_1$–$2p^2\,{}^1S_0$ *and* $2s2p\,{}^1P_1$–$2p^2\,{}^1D_2$ *transitions as function of* Z

	$2s^2\,{}^1S_0$–$2s2p\,{}^1P_1$		$2s2p\,{}^1P_1$–$2p^2\,{}^1S_0$		$2s2p\,{}^1P_1$–$2p^2\,{}^1D_2$	
Z	A_L	A_V	A_L	A_V	A_L	A_V
4	2.83 [8]	2.81 [8]	4.34 [8]	4.36 [8]	2.27 [6]	2.05 [6]
	5.4 ± 0.2 [8][a]					
5	8.20 [8]	8.17 [8]	1.14 [9]	1.14 [9]	5.23 [7]	5.08 [7]
	1.2 ± 0.1 [9][a]		1.2 ± 0.1 [9][g]		6.4 ± 0.3 [7][h]	
6	1.38 [9]	1.38 [9]	1.96 [9]	1.97 [9]	1.34 [8]	1.32 [8]
	1.8 ± 0.1 [9][a]		2.0 ± 0.3 [9][b]		1.39 ± 0.04 [9][b]	
7	1.94 [9]	1.94 [9]	2.84 [9]	2.85 [9]	2.29 [8]	2.26 [8]
	2.4 ± 0.1 [9][a]		2.9 ± 0.2 [9][c]		2.4 ± 0.2 [8][c]	
8	2.50 [9]	2.50 [9]	3.75 [9]	3.76 [9]	3.31 [8]	3.27 [8]
	3.0 ± 0.2 [9][a]		3.4 ± 0.2 [9][c]		3.4 ± 0.2 [8][c]	
9	3.06 [9]	3.07 [9]	4.68 [9]	4.69 [9]	4.38 [8]	4.35 [8]
	3.2 ± 0.3 [9][a]		4.8 ± 0.5 [9][e]		4.0 ± 0.2 [8][e]	
10	3.63 [9]	3.64 [9]	5.62 [9]	5.64 [9]	5.50 [8]	5.46 [8]
	4.3 ± 0.6 [9][a]					
11	4.21 [9]	4.22 [9]	6.59 [9]	6.61 [9]	6.67 [8]	6.63 [8]
12	4.80 [9]	4.82 [9]	7.59 [9]	7.60 [9]	7.90 [8]	7.87 [8]
	5.3 ± 0.4 [9][a]		7.4 ± 0.7 [9][d]		8.2 ± 0.6 [8][d]	
13	5.42 [9]	5.44 [9]	8.61 [9]	8.63 [9]	9.21 [8]	9.18 [8]
	5.2 ± 0.4 [9][a]		8.9 ± 0.8 [9][d]		9.3 ± 0.5 [8][d]	
14	6.06 [9]	6.08 [9]	9.68 [9]	9.70 [9]	1.06 [9]	1.06 [9]
	6.7 ± 0.5 [9][a]		1.0 ± 0.1 [10][f]		1.1 ± 0.1 [9][f]	
15	6.74 [9]	6.76 [9]	1.08 [10]	1.08 [10]	1.21 [9]	1.21 [9] [5]
	7.1 ± 0.4 [9][a]		1.1 ± 0.1 [10][d]		1.2 ± 0.1 [9][d]	
16	7.45 [9]	7.47 [9]	1.20 [10]	1.20 [10]	1.38 [9]	1.37 [9]
	7.7 ± 0.8 [9][a]		1.23 ± 0.04 [10][d]		1.4 ± 0.1 [9][d]	
17	8.21 [9]	8.23 [9]	1.32 [10]	1.32 [10]	1.56 [9]	1.56 [9]
	7.1 ± 0.4 [9][a]		1.2 ± 0.1 [10][k]		1.5 ± 0.1 [10][k]	
18	9.02 [9]	9.04 [9]	1.45 [10]	1.46 [10]	1.76 [9]	1.75 [9]
19	9.89 [9]	9.92 [9]	1.60 [10]	1.60 [10]	1.98 [9]	1.98 [9]
20	1.08 [10]	1.09 [10]	1.75 [10]	1.75 [10]	2.23 [9]	2.22 [9]
21	1.19 [10]	1.19 [10]	1.92 [10]	1.92 [10]	2.50 [9]	2.50 [9]
22	1.30 [10]	1.30 [10]	2.10 [10]	2.11 [10]	2.81 [9]	2.80 [9]
23	1.43 [10]	1.43 [10]	2.31 [10]	2.31 [10]	3.15 [9]	3.15 [9]
24	1.57 [10]	1.57 [10]	2.54 [10]	2.54 [10]	3.54 [9]	3.54 [9]
25	1.72 [10]	1.73 [10]	2.79 [10]	2.80 [10]	3.99 [9]	3.99 [9]
26	1.90 [10]	1.90 [10]	3.08 [10]	3.08 [10]	4.50 [9]	4.50 [9]
	2.0 ± 0.2 [10][a]		2.9 ± 0.3 [10][i]			
27	2.09 [10]	2.10 [10]	3.41 [10]	3.41 [10]	5.10 [9]	5.10 [9]
28	2.31 [10]	2.31 [10]	3.78 [10]	3.78 [10]	5.81 [9]	5.80 [9]
29	2.56 [10]	2.57 [10]	4.20 [10]	4.20 [10]	6.64 [9]	6.64 [9]
30	2.85 [10]	2.85 [10]	4.68 [10]	4.69 [10]	7.63 [9]	7.63 [9]
32	3.54 [10]	3.55 [10]	5.87 [10]	5.88 [10]	1.02 [10]	1.02 [10]
36	5.66 [10]	5.67 [10]	9.54 [10]	9.54 [10]	1.92 [10]	1.92 [10]
	5.7 ± 0.4 [9][a]		9.5 ± 0.8 [10][j]			
40	9.44 [10]	9.45 [10]	1.61 [11]	1.61 [11]	3.73 [10]	3.73 [10]
42	1.23 [11]	1.24 [11]	2.11 [11]	2.11 [11]	5.22 [10]	5.22 [10]
47	2.48 [11]	2.48 [11]	4.23 [11]	4.23 [11]	1.21 [11]	1.21 [11]
50	3.81 [11]	3.82 [11]	6.49 [11]	6.49 [11]	1.99 [11]	1.99 [11]
54	6.82 [11]	6.82 [11]	1.15 [12]	1.15 [12]	3.83 [11]	3.83 [11]
60	1.63 [12]	1.63 [12]	2.70 [12]	2.70 [12]	9.89 [11]	9.89 [11]
63	2.50 [12]	2.50 [12]	4.12 [12]	4.12 [12]	1.56 [12]	1.56 [12]
70	6.67 [12]	6.68 [12]	1.08 [13]	1.08 [13]	4.39 [12]	4.34 [12]
74	1.15 [13]	1.15 [13]	1.85 [13]	1.85 [13]	7.74 [12]	7.74 [12]
79	2.24 [13]	2.24 [13]	3.57 [13]	3.57 [13]	1.54 [13]	1.54 [13]
80	2.55 [13]	2.55 [13]	4.06 [13]	4.06 [13]	1.76 [13]	1.76 [13]
83	3.77 [13]	3.77 [13]	5.96 [13]	5.96 [13]	2.62 [13]	2.62 [13]
90	9.11 [13]	9.11 [13]	1.43 [14]	1.43 [14]	6.45 [13]	6.45 [13]
92	1.17 [14]	1.17 [14]	1.82 [14]	1.82 [14]	8.28 [13]	8.28 [13]
100	3.07 [14]	3.07 [14]	4.76 [14]	4.76 [14]	2.21 [14]	2.21 [14]

[a] [40].
[b] [41].
[c] [42].
[d] [43].
[e] [44].
[f] [45].
[g] [46].
[h] [47].
[i] [39].
[k] [48].
[k] [49].
[l] [50].

Table VII. *Transition probabilities (A in 10^8 s^{-1}) for resonance line* $2s^2\,{}^1S_0$–$2s2p\,{}^1P_1$ *calculated in length- and velocity-forms*

Z	A_L[a]	A_V[a]	A_L[b]	A_V[b]
5	9.43	9.39	11.9	12.0
6	14.9	14.8	17.6	17.6
7	20.4	20.4	23.0	23.2
8	25.8	25.9	28.6	28.6
10	37.0	37.1	39.7	39.5
12	48.6	48.7	51.3	50.8

[a] present result with experimental energies.
[b] [19].

different behavior of transition energies for the two transitions. The Z-dependence of the energy in Be-like ions was investigated in [38]. The energy difference for 2s–2p transitions is governed by the two leading terms, Z and $\alpha^2 Z^3$. The first of these dominates for small Z and the f-values are proportional to $1/Z$. With increasing Z, the second term becomes dominant and the f-values become proportional to Z. We can demonstrate these two behaviors for the f-values of two transitions: $2s2p\,{}^3P_0$–$2p^2\,{}^3P_1$ and $2s2p\,{}^3P_2$–$2p^2\,{}^3P_1$. The ratio of f-values for these transitions is about the ratio of their statistical weights 1 : 5 for $4 \leqslant Z \leqslant 32$. The f-values of the $2s2p\,{}^3P_0$–$2p^2\,{}^3P_1$ and $2s2p\,{}^3P_2$–$2p^2\,{}^3P_1$ transitions decrease by factors of 7 and 11, respectively, from $Z = 4$ to $Z = 32$. With increasing Z, the f-value of the second transition decreases also by a factor of 4 from $Z = 32$ to $Z = 100$, but the f-value of the first transition becomes larger by a factor of 4 from $Z = 32$ to $Z = 100$. This is caused by the increase of the energy difference for the $2s2p\,{}^3P_0$–$2p^2\,{}^3P_1$ transition by a factor of 1.4 for $Z = 32$ and a factor of 15 for $Z = 100$ in comparison with the $2s2p\,{}^3P_2$–$2p^2\,{}^3P_1$ transition.

Table VIII. *Lifetimes (τ in ps) for upper level* $2p^2\,{}^3P_J$ *as function of Z*

Z	${}^3P_0$	${}^3P_1$	${}^3P_2$	Expt.
4	2437	2437	2436	
5	1187	1186	1185	1240 ± 70[a]
6	779	778	777	790 ± 20[b]
7	580	579	578	650[c]
8	462	461	459	400 ± 40[d]
9	384	383	381	320 ± 40[e]
10	328	327	325	
11	286	284	282	
12	253	251	248	
13	227	224	220	
14	204	201	197	190 ± 15[f]
15	186	182	178	180 ± 10[g]
16	170	165	161	
17	156	151	147	160 ± 10[h]

[a] [46].
[b] [51].
[c] [52].
[d] [53].
[e] [44].
[f] [45].
[g] [43].
[h] [49].

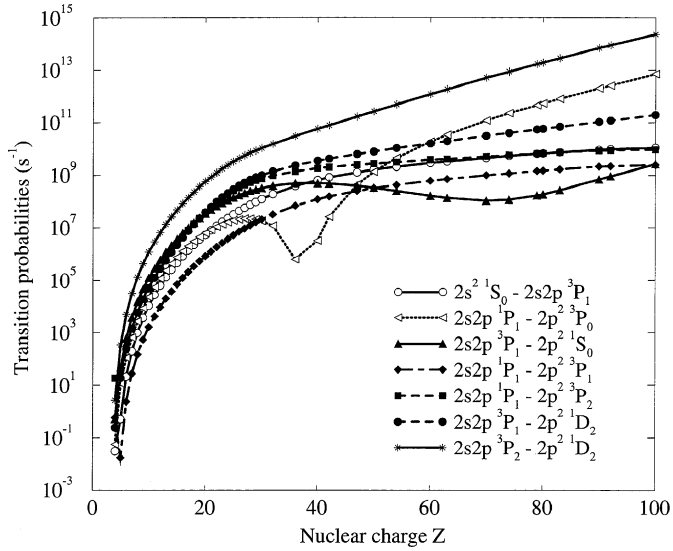

Fig. 4. Transition probabilities A for six intermediate coupling lines as functions of Z.

The Z-dependence of transition probabilities for the six singlet–triplet or triplet–singlet transitions $2s2p\,{}^1P_1$–$2p^2\,{}^3P_0$, $2s2p\,{}^3P_1$–$2p^2\,{}^1S_0$, $2s2p\,{}^1P_1$–$2p^2\,{}^3P_1$, $2s2p\,{}^1P_1$–$2p^2\,{}^3P_2$, $2s2p\,{}^3P_1$–$2p^2\,{}^1D_2$, and $2s2p\,{}^3P_2$–$2p^2\,{}^1D_1$ are shown in Fig. 4. The A-values for these transitions increase by a factor of 10^{+11} over the interval $4 \leqslant Z \leqslant 100$. It is known [59] that the ratios of A-values of LS-allowed and forbidden transitions are proportional to Z^6. We can see the minimum for $Z = 36$ for the A-values of the $2s2p\,{}^1P_1$–$2p^2\,{}^3P_0$ intercombination transition. This minimum is explained by the decrease of the energy interval between the $2s2p\,{}^1P_1$ and $2p^2\,{}^3P_0$ levels. For $Z = 32$, 36, and 40 the differences are equal to 164518 cm^{-1}, 64233 cm^{-1}, and -122283 cm^{-1}, respectively. The changes of sign means that the upper level is $2s2p\,{}^1P_1$ instead of $2p^2\,{}^3P_0$. It should be noted that our comments about LS-allowed and forbidden transitions refer primarily to ions with $Z < 36$. We can see from Fig. 4, that for $Z = 36$, the A-values for the all transitions except $2s2p\,{}^1P_1$–$2p^2\,{}^3P_0$ are in the range 10^7 s^{-1}–10^{10} s^{-1} and are comparable to A-values of allowed transitions (10^9 s^{-1}–10^{10} s^{-1} for $Z = 36$). The LS designation is meaningful for ions with small Z, but with increasing Z the jj designations become more appropriate.

4. Conclusion

We have presented a systematic second-order relativistic MBPT study of reduced matrix elements, oscillator strengths and transition rates for all 16 allowed and forbidden 2s–2p electric dipole transitions in berylliumlike ions with nuclear charges ranging from $Z = 4$ to 100. The retarded E1 matrix elements include correlation corrections from Coulomb and Breit interactions. Contributions from virtual electron–positron pairs were also included in the second-order matrix elements. Both length and velocity forms of the matrix elements were evaluated, and small differences, caused by the nonlocality of the starting HF potential, were found between the two forms. Second-order MBPT transition energies were used to evaluate oscillator strengths and transition rates. Our theoretical data for allowed transitions

agrees with experiment within the experimental error bars. We believe that these results will be helpful in analyzing old experiments and planning new ones. Additionally, the matrix elements from the present calculations provide basic theoretical input for calculations of reduced matrix elements, oscillator strengths and transition rates in three-electron boronlike ions.

Acknowledgements

The work of WRJ, MSS and AD was supported in part by National Science Foundation Grant No. PHY-95-13179. UIS acknowledges partial support by Grant No. B336454 from Lawrence Livermore National Laboratory. The authors owe to H.-S. Chou for helpful discussion.

References

1. Cohen, M. and Dalgarno, A., Proc. Roy. Soc. **A280**, 258 (1964).
2. Safronova, U. I., Ivanova, A. N. and Kharitonova, V. N., Theor. Exp. Chem. **5**, 325 (1969).
3. Dalgarno, A., Nucl. Instr. Meth. **110**, 183 (1973).
4. Victorov, D. C. and Safronova, U. I., J. Quant. Spectr. Radiat. Transfer **17**, 605 (1977).
5. Victorov, D. C. and Safronova, U. I., Opt. Spectrosc. **58**, 10 (1985).
6. Ralchenko, Yu. V. and Vainshtein, L. A., Phys. Rev. **A52**, 2449 (1995).
7. Safronova, U. I., Shlyaptseva, A. S., Kato, T., Masai, K. and Vainshtein, L. A., Atom. Data Nucl. Data Tables **60**, 1 (1995).
8. Victor, G. A. and Laughlin, C., Nucl. Instr. Meth. **110**, 189 (1973).
9. Nusbaumer, H., Astron. Astrophys. **16**, 77 (1972).
10. Eissner, W. B. and Tully, J. A., Astron. Astrophys. **253**, 625 (1992).
11. Sinanoğlu, O., Nucl. Instr. Meth. **110**, 193 (1973).
12. Nicolaides, C. N., Beck, D. R. and Sinanoğlu, O., J. Phys. B: At. Molec. Phys. **6**, 62 (1973).
13. Hibbert, A., J. Phys. B: At. Molec. Phys. **7**, 689 (1974).
14. Glass, R., J. Phys. B: At. Mol. Phys. **12**, 689 (1979).
15. Glass, R., J. Phys. B: At. Mol. Phys. **12**, 697 (1979).
16. Glass, R., Z. Phys. **A292**, 363 (1979).
17. Glass, R., Z. Phys. A – At. Nucl. **302**, 203 (1981).
18. Fleming, J., Hibbert, A. and Stafford, R. P., Physica Scripta **49**, 316 (1994).
19. Fleming, J., Vaeck, N., Hibbert, A., Bell, K. L. and Godefroid, M. R., Physica Scripta **53**, 446 (1996).
20. Wiese, W. L. and Weiss, A. W., Phys. Rev. **175**, 50 (1968).
21. Weiss, A. W., Nucl. Instr. Meth. **90**, 121 (1970).
22. Fawcett, B. C., Atom. Data Nucl. Data Tables **22**, 473 (1978).
23. Froese Fisher, C., Physica Scripta **49**, 323 (1994).
24. Fleming, J. *et al.*, Astr. J. **455**, 758 (1995).
25. Weiss, A. W., Phys. Rev. **A51**, 1067 (1995).
26. Froese Fisher, C. and Gaigalas, G., Physica Scripta **56**, 436 (1997).
27. Tully, J. A., Seaton, M. J. and Berrington, K. A., J. Phys. B: At. Mol. Phys. **23**, 3811 (1990).
28. Verner, D. A., Verner, E. M. and Ferland, G. J., At. Data Nucl. Data Tables **64**, 1 (1996).
29. Kim, Y.-Ki and Desclaux, J. P., Phys. Rev. Lett. **36**, 139 (1976).
30. Armstrong, Jr. L., Fielder, W. R. and Lin, D. L., Phys. Rev. **A14**, 1114 (1976).
31. Cheng, K. T. and Johnson, W. R., Phys. Rev. **A15**, 1326 (1977).
32. Lin, C. D. and Johnson, W. R., Phys. Rev. **A15**, 1046 (1977).
33. Cheng, K. T., Kim, Y.-Ki and Desclaux, J. P., At. Data Nucl. Data Tables **24**, 111 (1979).
34. Ynnerman, A. and Froese Fisher, C., Phys. Rev. **A51**, 2020 (1995).
35. Ynnerman, A. and Froese Fisher, C., Z. Phys. **D34**, 1 (1995).
36. Johnson, W. R., Plante, D. R. and Sapirstein, J., Adv. At. Mol. Opt. Phys. **35**, 255 (1995).
37. Johnson, W. R., Liu, Z. W. and Sapirstein, J., At. Data Nucl. Data Tables **64**, 279 (1996).
38. Safronova, M. S., Johnson, W. R. and Safronova, U. I., Phys. Rev. **53**, 4036 (1996).
39. Chen, M. H., Cheng, K. T. and Johnson, W. R., Phys. Rev. **A47**, 3692 (1993).
40. Buchet, J. P. *et al.*, Phys. Rev. **A30**, 309 (1984).
41. Curtis, L. J. and Ellis, D. G., J. Phys. B: At. Mol. Phys. **29**, 645 (1996).
42. Reistad, N., Hutton, R., Nilson, A. E., Martinson, I. and Mannervik, S., Physica Scripta **34**, 151 (1986).
43. Engström, L. *et al.*, Physica Scripta **24**, 551 (1981).
44. Träbert, E. and Heckmann, P. H., Physica Scripta **22**, 489 (1980).
45. Knystautas, E. J., Buchet–Poulizac, M. C., Buchet, J. P. and Druetta, M., J. Opt. Soc. Am. **69**, 474 (1979).
46. Träbert, E., Heckmann, P. H. and Buttlar, H. V., Z. Phys. **A281**, 333 (1977).
47. Kernahan, J. A., Pinnigton, E. H., Livingston, A. E. and Irwin, D. J. G., Physica Scripta **12**, 319 (1975).
48. Bergström, I., Bromander, J., Buchta, R., Lundin, L. and Martinson, I., Phys. Lett. **A28**, 721 (1969).
49. Träbert, E. *et al.*, Phys. Lett. **A202**, 91 (1995).
50. Kawatsura, K. *et al.*, Nucl. Instr. Meth. **A262**, 150 (1987).
51. Doerfert, J., Träbert, E., Wolf, A., Schwalm, D. and Uwira, O., Phys. Rev. Lett. **78**, 4355 (1997).
52. Pegg, D. J., Chupp, E. L. and Dotchin, L. W., Nucl. Instr. Meth. **90**, 71 (1970).
53. Buchet, J. P., Poulizac, M. C. and Carre, M., J. Opt. Soc. Am. **62**, 623 (1972).
54. Buchet, J. P., Buchet-Poulizac, M. C. and Druetta, M., J. Opt. Soc. Am. **66**, 842 (1976).
55. Garstang, R. H. and Shamey, L. J., Astrophys. J. **148**, 665 (1967).
56. Smith, M. W., Martin, G. A. and Wiese, W. L., Nucl. Instr. Meth. **110**, 219 (1973).
57. Reistad, N. and Martinson, I., Phys. Rev. **A34**, 2632 (1986).
58. Träbert, E., Z. Phys. D – At. Mol. Clusters **9**, 143 (1988).
59. Safronova, U. I. and Rudzikas, Z. B., J. Phys. B: At. Mol. Phys. **10**, 7 (1977).

